THE JOURNAL OF BIOLOGICAL CHEMISTRY
Vol. 280, No. 22, Issue of June 3, pp. 21313–21320, 2005
Printed in U.S.A.

Mouse Sir2 Homolog SIRT6 Is a Nuclear ADP-ribosyltransferase*

Received for publication, November 24, 2004, and in revised form, March 22, 2005
Published, JBC Papers in Press, March 28, 2005, DOI 10.1074/jbc.M413296200

Gregory Liszt‡, Ethan Ford‡, Martin Kurtev, and Leonard Guarente§

From the Department of Biology, Massachusetts Institute of Technology, Cambridge, Massachusetts 02139

Members of the Sir2 family of NAD-dependent protein deacetylases regulate diverse cellular processes including aging, gene silencing, and cellular differentiation. Here, we report that the distant mammalian Sir2 homolog SIRT6 is a broadly expressed, predominantly nuclear protein. Northern analysis of embryonic samples and multiple adult tissues revealed mouse SIRT6 (mSIRT6) mRNA peaks at day E11, persisting into adulthood in all eight tissues examined. At the protein level, mSIRT6 was readily detectable in the same eight tissue types, with the highest levels in muscle, brain, and heart. Subcellular localization studies using both C- and N-terminal green fluorescent protein fusion proteins showed mSIRT6-green fluorescent protein to be a predominantly nuclear protein. Indirect immunofluorescence using antibodies to two different mSIRT6 epitopes confirmed that endogenous mSIRT6 is also largely nuclear. Consistent with previous findings, we did not observe any NAD^+-dependent protein deacetylase activity in preparations of mSIRT6. However, purified recombinant mSIRT6 did catalyze the robust transfer of radiolabel from [^{32}P]NAD to mSIRT6. Two highly conserved residues within the catalytic core of the protein were required for this reaction. This reaction is most likely mono-ADP-ribosylation because only the modified form of the protein was recognized by an antibody specific to mono-ADP-ribose. Surprisingly, we observed that the catalytic mechanism of this reaction is intra-molecular, with individual molecules of mSIRT6 directing their own modification. These results provide the first characterization of a Sir2 protein from phylogenetic class IV.

Members of the Sir2 family of enzymes, conserved from bacteria to man, utilize oxidized NAD^+ as a cosubstrate in the deacetylation of a wide variety of proteins, thereby regulating diverse processes including aging, genomic silencing, recombination, cell fate, and metabolism (1). In yeast, the archetypal Sir2p localizes to chromatin sites at the telomeres, ribosomal DNA, and silent mating type loci, facilitating genomic silencing through the deacetylation of lysines within the histone H3 and H4 tails (2). In this context, yeast Sir2p promotes mother cell longevity by repressing ribosomal DNA recombination and formation of toxic extra-chromosomal ribosomal DNA circles (3, 4). Overexpression of Sir2p extends yeast life span (5), and Sir2p activity increases in response to caloric restriction (6), contributing to the resultant extension of life span (7). Intriguingly, Sir2 orthologs in worm and fly also promote longevity, although probably by different molecular mechanisms (8–10).

Mammalian genomes contain seven Sir2 homologs, termed sirtuins (SIRTs). Of these, SIRT1, orthologous to the yeast Sir2, is the best characterized and has the broadest substrate specificity (11). A nuclear protein, SIRT1 deacetylates several substrates *in vivo*, including MyoD, p53, and FOXO transcription factors, thereby affecting cell differentiation and survival under stress (11–13). Recently, mouse SIRT1 was reported to inhibit the mobilization of fatty acids in white adipose tissue by repressing PPARγ, linking Sir2 proteins to the physiology of caloric restriction in mammals (14).

Of the remaining SIRTs (SIRT2–7), an *in vivo* substrate has only been identified for the cytoplasmic SIRT2 (15). This substrate, β-tubulin, is specifically deacetylated by SIRT2 (15), although the biological consequences of this reaction are unclear.

Yeast Sir2 and its orthologs, including mouse SIRT1 and bacterial CobB, catalyze the tightly coupled cleavage of NAD^+ and protein deacetylation, producing nicotinamide and 2-*O*-acetyl-ADP-ribose reaction products (16). Whereas Sir2 proteins are generally thought to be NAD-dependent protein deacetylases, most also display a less robust mono-ADP-ribosyltransferase activity *in vitro* (17–20). Mutations in phylogenetically conserved residues within the catalytic core of Sir2 and SIRT1 have failed to separate the two enzymatic activities (21). The initial observation that ADP-ribosylation by Sir2 is stronger on acetylated substrates (22), combined with subsequent mechanistic studies (18, 20), has led to the conclusion that the deacetylase and phosphoribosyltransferase activities of Sir2 proteins are coupled (16).

Using sequence similarity, eukaryotic Sir2 genes have been divided into four broad phylogenetic classes (23), known as classes I–IV (Fig. 1). SIRT1, SIRT2, and SIRT3 are class I, SIRT4 is class II, and SIRT5 falls within the predominantly prokaryotic class III. Finally, mammalian SIRT6 and SIRT7 are class IV sirtuins (23). *In vitro* studies indicate that human SIRT1, SIRT2, SIRT3, and SIRT5 possess NAD-dependent histone deacetylase activity (15), whereas SIRT4, SIRT6, and SIRT7 fail to deacetylate ^{3}H-labeled acetylated histone H4 peptide (15). The lack of detectable deacetylase activity in these SIRTs may result from their specificity for targets other than those tested, or it may indicate an enzymatic activity other than deacetylation inherent in these sirtuins.

Mono-ADP-ribosylation is emerging as a common mechanism of reversible protein modification within mammalian cells. Originally described as the acting mechanism for specific bacterial toxins, ADP-ribosylation is typically performed by separate families of intra- and extracellular enzymes in vertebrates (24). Known targets of the intracellular class of enzymes include molecular chaperone GRP78/BiP, translational elongation factor 2, and β-subunit of heterotrimeric G-proteins (24). Extracellular mammalian ADP-ribosyltransferases, generally found in cells of the immune system, modify substrates important for the im-

* The costs of publication of this article were defrayed in part by the payment of page charges. This article must therefore be hereby marked "*advertisement*" in accordance with 18 U.S.C. Section 1734 solely to indicate this fact.

‡ Both authors contributed equally to this work.

§ To whom correspondence should be addressed: Dept. of Biology, Massachusetts Institute of Technology, 77 Massachusetts Ave., Rm. 68-280, Cambridge, MA 02139. Tel.: 617-253-6965; Fax: 617-452-4130; E-mail: leng@mit.edu.

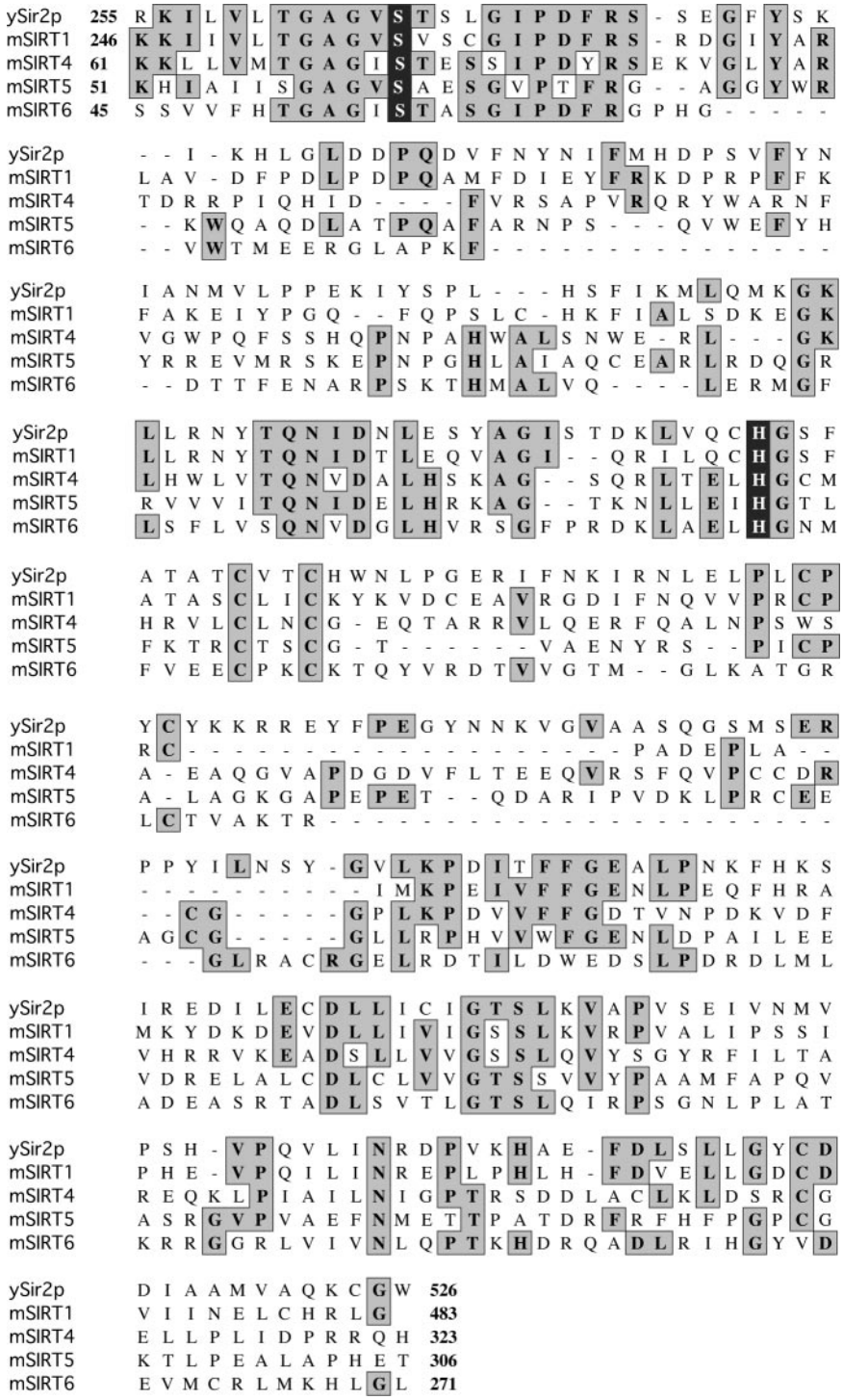

FIG. 1. **Sequence alignment of mouse sirtuin core domains.** Conserved core domains of mouse SIRT1, SIRT4, SIRT5, and SIRT6 were aligned with the yeast Sir2 core using ClustalW. In the sirtuin phylogenetic tree, SIRT1 is class I, SIRT4 is class II, SIRT5 is class III, and SIRT6 is class IV. At each position of the alignment, identical residues are *boxed* and *shaded* in *gray*. Amino acids *boxed* in *black* correspond to mSIRT6 residues targeted for mutagenesis in this study.

mune response, as well as integrin $\alpha 7$ and the antimicrobial peptide defensin (24). In most known cases, ADP-ribosylation of arginine residues results in reversible inactivation of the substrate protein (25), although this modification may enhance certain enzymatic functions within the substrate (26).

In this report, we characterize the tissue-specific expression, subcellular localization, and *in vitro* enzymatic activity of mouse SIRT6. This investigation, the first detailed study of a class IV sirtuin, reveals mouse SIRT6 to be a widely expressed, predominantly nuclear protein with a robust auto-ADP-ribosyltransferase activity.

MATERIALS AND METHODS

Multiple Sequence Alignments—Sequences of mouse proteins SIRT1, SIRT4, SIRT5, and SIRT6, as well as yeast Sir2p, were obtained from the Proteome BioKnowledge® Library (proteome.incyte.com/control/tools/proteome). Core domains were aligned by ClustalW using software from the DNASTAR package.

Plasmid Construction—IMAGE clone 1259892, which contains the mouse SIRT6 cDNA, was obtained from American Type Culture Collection. The mSIRT6[1] coding sequence was amplified by PCR and cloned into the EcoRI and BamHI sites of pEGFP-N1 and the BglII and EcoRI sites of pEGFP-C2, creating pmSIRT6-EGFP and pEGFP-mSIRT6, respectively. Similarly, the mSIRT6 coding sequence was amplified by PCR and cloned into the NheI and BamHI sites of pET28a (Novagen) and pET-GST (a gift from Robert Marciniak) creating pET28a-His$_6$-

[1] The abbreviations used are: mSIRT6, mouse SIRT6; GFP, green fluorescent protein; EGFP, enhanced green fluorescent protein; DAPI, 4′,6-diamidino-2-phenyindole; PBS, phosphate-buffered saline; GST, glutathione *S*-transferase.

SIRT6 and pET-GST-SIRT6. pET28a-His_6-mSIRT6-S56A and pET28a-His_6-SIRT6-H133Y were created using the Stratagene QuikChange site-directed mutagenesis kit according to the manufacturer's instructions. PET-GST-SIRT6-(274–355) was created by amplifying the portion of the mSIRT6 cDNA corresponding to amino acids 274–355 and ligating it into pET-GST cut with NheI and BamHI.

Multiple Tissue Northern Blots—Probe containing the SIRT6 open reading frame was created using the PrimeIt Random Primer Labeling kit (Stratagene) according to the manufacturer's instructions. This ^{32}P-labeled fragment was used to probe Stratagene Multiple Tissue Northern Blots according to the manufacturer's instructions. The blots were then stripped and reprobed with the actin probe included in the kit.

Antibody Production—pET28a-His_6-mSIRT6 and pET-GST-mSIRT6-(274–355) were transformed into BL21(DE3)-Codon Plus-RP cells (Stratagene) and inoculated into 4- or 2-liter cultures of LB (50 mg/ml kanamycin and 35 mg/ml chloramphenicol), respectively. The cells were grown at 37 °C to an optical density of 0.7. Protein expression was induced by the addition of isopropyl 1-thio-β-D-galactopyranoside to a final concentration of 0.4 mM for 2 h, and the cells were harvested by centrifugation.

The cells containing the pET28a-His_6-mSIRT6 plasmid were resuspended in lysis buffer (0.1 M NaH_2PO_4, 10 mM Tris, 8 M urea, pH 8.0) and lysed by freezing in liquid N_2. The lysate was centrifuged at 19,000 rpm in a Sorvall SS-34 rotor. The supernatant was incubated with 4 ml of nickel-nitrilotriacetic acid-agarose (Stratagene) for 3 h at 4 °C, loaded onto a column, and washed extensively with wash buffer (0.1 M NaH_2PO_4, 10 mM Tris, 8 M urea, pH 6.4). The purified protein was eluted with elution buffer (0.1 M NaH_2PO_4, 10 mM Tris, 8 M urea, pH 3.0) in 1.5-ml fractions. The pH was neutralized by the immediate addition of 100 μl of 1 M Tris base. The fractions containing protein were pooled and dialyzed against PBS. This protein was sent to Covance Reseach Bioproducts for antibody production.

The cells containing the pET-GST-SIRT6-(274–355) plasmid were resuspended in PBSTG (PBS, 0.1% Tween 20, 10% glycerol, 1 mM dithiothreitol) and 0.1 g of lysozyme, incubated at 37 °C for 20 min, and frozen in liquid N_2. The lysis was completed by sonication, and the lysate was centrifuged at 19,000 rpm for 30 min. The supernatant was incubated with 4 ml of GST-agarose (Sigma) for 3 h at 4 °C and loaded onto a column. The column was washed extensively with PBSTG, and the protein was eluted with elution buffer (50 mM Tris, 10 mM glutathione, pH 7.5). Fractions containing protein were dialyzed against PBS and sent to Covance Reseach Bioproducts for antibody production.

The antibodies were affinity-purified as follows. Aliquots of the proteins used to generate the antibodies were attached to1 ml of NHS-activated Sepharose columns (Amersham Biosciences) according to the manufacturer's instructions. 10 ml of the final bleed of each antibody was combined with 10 ml of antibody wash buffer (20 mM Hepes, pH 7.5, 150 mM NaCl, 0.1% Tween 20) and applied to the column. Each column was washed extensively with antibody wash buffer, and the antibody was eluted with 100 mM glycine, pH 2.5. The pH was neutralized by the addition of 0.1 volume of 1 M Hepes-KOH, pH 7.5. The antibodies were then subjected to a second round of affinity purification, but this time the anti-mSIRT6 (full-length) antibody was applied to the SIRT6-(274–355) column, and the anti-mSIRT6-(274–355) antibody was applied to the SIRT6 (full length) column.

Western Blot Analysis—Homogenized mouse tissues from four mice of the FVB genetic background were obtained as a generous gift from L. Bordone (Massachusetts Institute of Technology). From these samples, SDS-solubilized proteins were prepared (27), equal amounts of which were used for Western analysis.

For Western detection, samples were resolved on 4–15% Tris-HCl gradient gels (Bio-Rad), transferred to polyvinylidene difluoride membrane, and blocked using 4% nonfat dry milk in PBS with 0.1% Tween 20 (PBS-T). Primary anti-mSIRT6 antibody was diluted 1:400 in PBS-T before incubation with membranes. Rabbit anti-ADP-ribose antibody (27), a generous gift from H. Hilz, was used at a 1:100 dilution in PBS-T. Anti-actin C4 (Sigma) was used as a loading control (1:5000) in multiple tissue Western blots. Secondary antibodies were goat anti-rabbit or sheep anti-mouse horseradish peroxidase-conjugated antibodies (1:10,000). Chemiluminescent detection was achieved by incubation with the ECL reagent (Amersham Biosciences).

Immunofluorescence and GFP Microscopy—NIH 3T3 cells were grown in Dulbecco's modified Eagle's medium for 48 h on gelatin-treated 18-mm circular glass coverslips in 6-well plates. Cells were fixed for 10 min with 4% paraformaldehyde, washed twice with PBS, and then permeabilized by a 3-min treatment with 0.2% Triton X-100. Coverslips were gently washed twice with PBS and blocked with 10% bovine serum albumin for 15 min, transferred to a rack, and washed in PBS. Affinity-purified primary antibody was added at a 1:100 dilution. Staining proceeded for 45 min, and cells were then washed twice for 5 min in fresh PBS. Fluorescein isothiocyanate-conjugated chicken anti-rabbit IgG was diluted in 1% bovine serum albumin and incubated with coverslips for 45 min. Coverslips were mounted with VectaShield mounting media containing 4′,6-diamidino-2-phenyindole, dilactate (Vector, Burlingame, CA). Microscopy was performed on a Nikon Eclipse E500 fluorescence microscope. Digital images were obtained using a SPOT RT charge-coupled device camera and software using identical exposure times for comparable samples.

NIH 3T3 cells were transfected with 5 μg of each GFP construct using FuGENE 6 (Roche Applied Science) according to manufacturer's instructions. Cells were grown for 48 h on glass coverslips. Samples were fixed, DAPI-stained, and visualized as described above.

Purification of Recombinant SIRT6 Protein—BL21(DE3)-Codon Plus-RP *Escherichia coli* (Stratagene) were transformed with the mSIRT6 expression plasmids. Protein purifications were performed essentially as described for antibody purification. Briefly, fusion protein expression was induced in 0.4 mM isopropyl 1-thio-β-D-galactopyranoside at 37 °C for 1 h. The induced His_6-tagged proteins were purified with nickel-nitrilotriacetic acid-agarose beads (Qiagen) under native conditions. The control eluate was prepared from a bacterial clone carrying pET28a vector alone. GST-tagged proteins were purified by a similar method, with affinity purification accomplished with glutathione-agarose beads (Pierce). Control eluate for GST-tagged proteins was prepared from bacteria carrying pET28-GST. Aliquots of recombinant proteins were stored at −70 °C.

ADP-ribosylation Assays and Detection of ADP-ribosylated Proteins—ADP-ribosylation assays were performed essentially as described previously (22), with minor modifications. Reactions were performed in a 50-μl total volume containing 5 μg of recombinant SIRT6 in 50 mM Tris-HCl, pH 8.0 (at 22 °C), 150 mM NaCl, 10 mM dithiothreitol, 1 μM unlabeled NAD, and 8 μCi of [^{32}P]NAD (800 Ci mmol^{-1}; Amersham Biosciences). Reactions also contained 2.5 μg of core histones as indicated. For reactions containing both His_6-tagged and GST-tagged recombinant SIRT6 protein, 2.5 μg of each protein was added. Prior to SDS-PAGE analysis, all reactions were purified from unincorporated [^{32}P]NAD using Micro Bio-Spin chromatography columns (Bio-Rad) with a 6000-Da exclusion limit. Gels were transferred to polyvinylidene difluoride membrane before autoradiography and subsequent immunoblot analysis. Blots were stained with Coomassie Blue, and the Coomassie Blue-stained bands and Western signals were aligned to verify that the radioactive bands were SIRT6.

Quantitation of ADP-ribosylation—ADP-ribosylation reactions were performed as described above, but with the following modifications. Total reaction volume was 40 μl, including ~0.5 μg of protein, 0.8 μl of 6.25 μM [^{32}P]NAD, and 4 μl of 10 μM NAD. Purified reaction products were separated by SDS-PAGE, and bovine serum albumin standards of 5, 2, 0.8, 0.4, and 0.1 μg were included on the same gel. SIRT6 protein concentrations in each lane were determined by comparison with these standards upon Coomassie Blue staining. Gel was analyzed by autoradiography, and radioactive SIRT6 bands were excised. Radioactivity was determined by scintillation counting on a Beckman LS 6500 Liquid Scintillation Counter. A standard curve relating NAD quantity to radioactivity was generated by scintillation counting of known pmol quantities of [^{32}P]NAD diluted to reflect the ratio of unlabeled to labeled NAD in the original reaction. This curve was used to estimate pmol of NAD incorporated in SIRT6 bands. For each band, pmol of NAD was divided by pmol of SIRT6. This final value reflects the molar ratio of total incorporated ADP-ribose to SIRT6.

RESULTS

mSIRT6 Expression in Mice and Embryos—To determine the expression pattern of mSIRT6, we analyzed RNA extracts from eight adult mouse tissues by Northern blotting (Fig. 2*A*). Using a cDNA probe corresponding to the 5′ region of mSIRT6, expression of mSIRT6 mRNA was observed in every tissue type tested (Fig. 2*A*). Confirming the predictions of sequence analysis (23), mSIRT6 was detected as a single 1.0-kb transcript, suggesting that this gene is not found in alternate splice forms. When normalized to actin, the highest levels of mSIRT6 mRNA were seen in the brain, heart, and liver, with the lowest expression level observed in skeletal muscle.

To evaluate mSIRT6 levels during development, we probed Northern blots of RNA from four mouse embryonic stages from

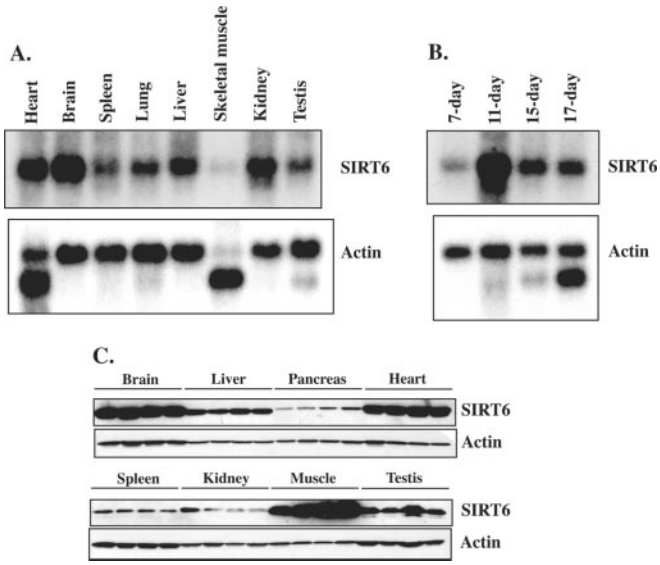

FIG. 2. **Analysis of mouse SIRT6 and actin expression in adult tissues and developing embryos.** *A*, RNA was isolated from the indicated tissues in wild-type adult mice, resolved by electrophoresis, and subjected to Northern blotting. Blots were probed with ^{32}P-labeled cDNA specific to mSIRT6 (*top panel*) or actin (*bottom panel*). Muscle actin found in heart and skeletal muscle samples migrated as a distinct band. *B*, RNA from 7-, 11-, 15-, and 17-day mouse embryos was analyzed by Northern blotting as described in *A*. *C*, protein extracts from the indicated wild-type mouse tissues were resolved by SDS-PAGE and analyzed by Western blotting using antibodies specific to mSIRT6 (*top panel*) or actin (*bottom panel*). For each tissue type, samples from four different mice were included.

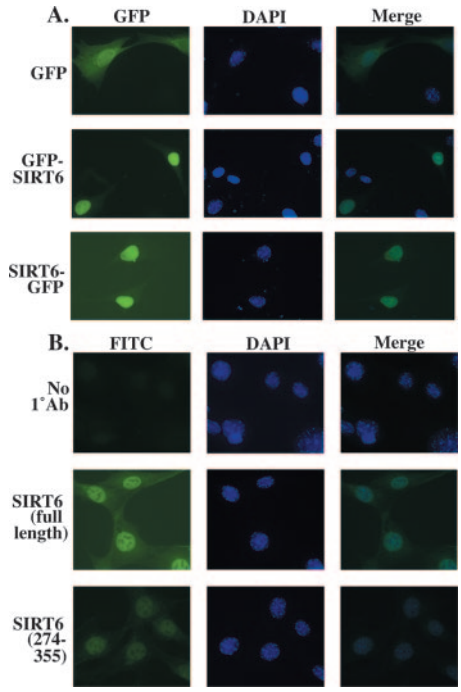

FIG. 3. **Subcellular localization of mSIRT6 by GFP and indirect immunofluorescence microscopy.** *A*, NIH 3T3 cells were transfected with GFP (*top row*), an N-terminal GFP-mSIRT6 fusion (*middle row*), or a C-terminal mSIRT6-EGFP fusion (*bottom row*). Transfections were performed on glass coverslips in 6-well plates. 48 h after transfection, cells were washed, fixed with paraformaldehyde, stained with DAPI, and analyzed by fluorescence microscopy. The fluorescein isothiocyanate channel (*left column*) shows GFP fluorescence, and the DAPI channel (*middle column*) reveals nucleic acid localization. Images from both channels are merged in the *right column*. For each transfection, a representative field of cells is pictured. *B*, NIH 3T3 cells grown on coverslips were stained with affinity-purified rabbit polyclonal antibodies to two different mSIRT6 epitopes (full-length mSIRT6, *middle row*; mSIRT6 amino acids 274–355, *bottom row*). Samples were then stained with DAPI and Cy3-conjugated anti-rabbit IgG and visualized by fluorescence microscopy. Cy3 fluorescence is shown in the *left column*, DAPI-stained nucleic acids are shown in the *middle column*, and the merged image is shown in the *right column*.

embryonic day E7 to E17 (Fig. 2*B*). Mouse SIRT6 transcript was readily detectable in all embryonic samples, reaching a peak at E11.

Having established the prevalence of mSIRT6 message in embryonic and adult tissues, we wished to determine the distribution of mSIRT6 protein. Affinity-purified antiserum specific to mSIRT6 was used to probe Western blots of proteins isolated from eight adult murine tissue types (Fig. 2*C*). For each tissue type, samples from four individual animals were obtained and analyzed by immunoblot. As illustrated in Fig. 2*C*, mSIRT6 protein was detectable in all tissue types as a single 40-kDa band. As expected from Northern analysis, levels were high in brain, liver, and heart when normalized to actin protein levels. Surprisingly, mSIRT6 protein was most strongly expressed in muscle (Fig. 2*C*), despite the relative paucity of its transcript in this tissue. This observation might indicate increased mSIRT6 transcript stability in muscle or an enhanced rate of translation in this tissue type relative to others tested.

Visualization of mSIRT6-GFP in Nuclei—In order to observe the subcellular localization of mSIRT6, we engineered two GFP fusion expression vectors under the control of the cytomegalovirus promoter. Both a C-terminal (mSIRT6-GFP) and an N-terminal (GFP-mSIRT6) fusion construct were transfected into NIH 3T3 cells grown on glass coverslips. Samples were cultured for 48 h, at which point they were fixed, washed, and DAPI-stained to reveal nucleic acids. Fluorescence microscopy of cells harboring each GFP fusion construct showed strong localization of mSIRT6-GFP to the nucleus, accompanied by diffuse cytoplasmic staining, as judged by colocalization of DAPI-stained nuclei (Fig. 3*A*). As expected, transfection of GFP alone caused intense fluorescence throughout the cytoplasm and nucleus.

Indirect Immunofluorescence of mSIRT6—To visualize endogenous levels of mSIRT6, affinity-purified rabbit antisera to two different mSIRT6 antigens were used to probe NIH 3T3 cells by indirect immunofluorescence. As a control, cells were incubated without primary antibody and subsequently stained with DAPI and Cy3-conjugated anti-rabbit IgG. Very faint background staining was seen throughout the cytoplasm and nucleus in these control samples (Fig. 3*B*). Strikingly, mSIRT6 showed strong staining predominantly in the nucleus (Fig. 3*B*), regardless of which anti-mSIRT6 antibody was used in the primary incubation. In both cases, endogenous mSIRT6 appeared to be excluded from the nucleolus.

Importantly, immunofluorescence and GFP localization studies revealed the same predominantly nuclear localization pattern for mSIRT6. We therefore conclude that the majority of mSIRT6 is found in the nucleus, whereas a small fraction may be localized to the cytoplasm.

mSIRT6 Catalyzes the Transfer of ^{32}P from a ^{32}P-labeled NAD Donor—Of the seven mammalian Sir2 homologs, only SIRT1, SIRT2, SIRT3, and SIRT5 have been shown to have NAD^+-dependent protein deacetylase activity *in vitro* (15). Consistent with published reports, we did not observe any protein deacetylase activity of mouse or human SIRT6 using a variety of experimental conditions and potential substrates (data not shown).

Several sirtuins also possess a mono-ADP-ribosyltransferase activity (19). We therefore sought to test whether mSIRT6 could catalyze the transfer of radiolabel from [^{32}P]NAD^+ to histones, an assay of ADP-ribosyltransferase activity. His_6-

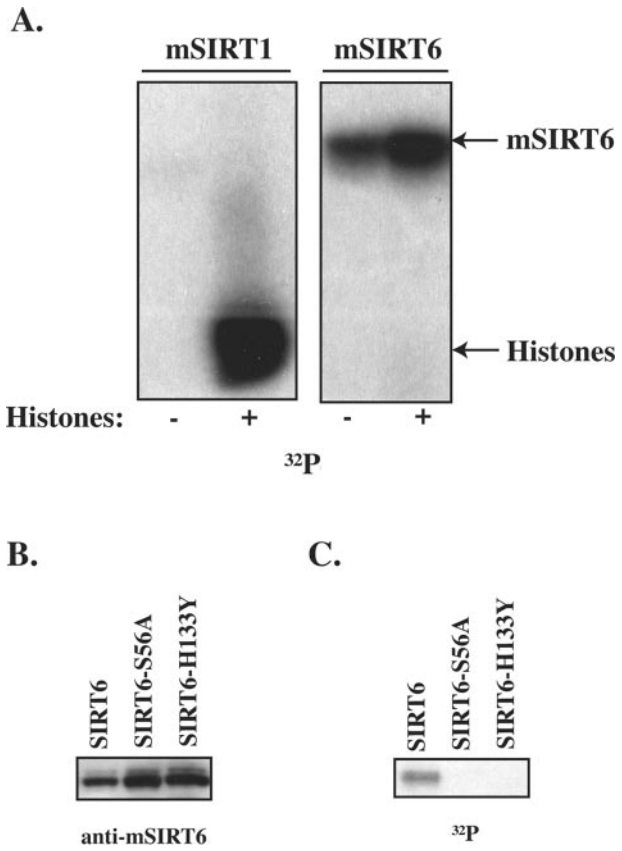

FIG. 4. **NAD$^+$-dependent modification of mSIRT6.** *A*, recombinant hSIRT1 (*left panel*) and mSIRT6 (*right panel*) were incubated in the presence of [^{32}P]NAD$^+$ with and without core histones. Samples were purified by gel filtration chromatography, subjected to SDS-PAGE, and exposed to film for 2 h. *B* and *C*, wild-type and two mutant forms of mSIRT6 (S56A and H133Y) were incubated with [^{32}P]NAD$^+$, purified, and resolved by SDS-PAGE. Proteins were transferred to nitrocellulose membrane and developed by autoradiography (*C*). The presence of wild-type and mutant SIRT6 was confirmed by probing membrane with affinity-purified anti-mSIRT6 rabbit polyclonal antibody (*B*).

tagged human SIRT1 and mSIRT6 were expressed in *E. coli* and purified by chromatography. Equal amounts of hSIRT1 and mSIRT6 were incubated with [^{32}P]NAD$^+$ in the presence and absence of core histones (Fig. 4*A*). Whereas hSIRT1 transferred label efficiently to histones, mSIRT6 failed to do so (Fig. 4*A*). However, mSIRT6 catalyzed the robust transfer of label to itself, regardless of whether histones were present in the reaction (Fig. 4*A*). Control extracts purified from *E. coli* containing vector alone possessed no detectable activity under these conditions (data not shown).

We wished to determine whether ^{32}P transfer stimulated by mSIRT6 required the catalytic activity of the enzyme. Two point mutations in highly conserved residues within the mSIRT6 core domain were introduced by site-directed mutagenesis (Fig. 1). The histidine residue at position 133 was changed to tyrosine (mSIRT6-H133Y), a mutation previously demonstrated to abolish enzymatic activity in human and yeast Sir2 proteins (17, 19). In a separate construct, the phylogenetically invariant serine residue at position 56 was mutated to alanine (mSIRT6-S56A). Serine 56 is buried deep in the active site of the enzyme and does not appear to be structurally important (28). Both mutant proteins were expressed in *E. coli*, purified, and incubated in the presence of [^{32}P]NAD$^+$ as described above. Unincorporated NAD was removed by chromatography column. Proteins were separated by SDS-PAGE, transferred to nitrocellulose membrane, and exposed to film. Whereas wild-type mSIRT6 efficiently transferred ^{32}P radiolabel to itself, no label transfer was detected in mutants mSIRT6-S56A and mSIRT6-H133Y (Fig. 4*C*). The presence of mutant proteins on the membrane was verified by Western blotting using affinity-purified antibody to mSIRT6 (Fig. 4*B*).

Based on this requirement for two catalytic core residues, we conclude that mSIRT6 catalyzes the transfer of radiolabel from [^{32}P]NAD by an enzymatic mechanism.

Labeling of proteins with [^{32}P]NAD$^+$ can also occur nonenzymatically by the covalent binding of NAD. Such labeling, as observed in the case of glyceraldehyde-3-phosphate dehydrogenase (29), can be misinterpreted as ADP-ribosylation of specific amino acid acceptors (29, 30). We have observed low levels of nonspecific radiolabeling of proteins incubated in the presence of [^{32}P]NAD$^+$. Under our reaction conditions, such modification occurs in core histones and enzymatically inactive Sir2 point mutants, generally not labeling >0.001% of total protein after a 1-h incubation at 30 °C (Fig. 5), as determined by scintillation counting of protein bands. In contrast, in the case of mSIRT6, we observed incorporation of a molar quantity of ADP-ribose equivalent to 15% of total moles of mSIRT6 present in the reaction (Fig. 5). For this reason, and because of the difference in labeling efficiency between wild-type and point-mutant varieties of mSIRT6, we conclude that the transfer of ^{32}P radiolabel occurs via a robust enzymatic mechanism.

Auto-ADP-ribosylation of mSIRT6—To test the hypothesis that mSIRT6 catalyzed the mono-ADP-ribosylation of itself, we probed the reaction products from the above label transfer reactions with an antibody specific to mono-ADP-ribose (31). This antibody recognized a band corresponding to the radiolabeled mSIRT6 following incubation with [^{32}P]NAD (Fig. 6*A*). No band was present at the corresponding position in preparations from mutant mSIRT6 (Fig. 6*A*), demonstrating the specificity of the antibody for the modified form of mSIRT6. This evidence strongly suggests that this modified form of mSIRT6 is mono-ADP-ribosylated. Whereas our results do not rule out the possibility that the modification of wild-type mSIRT6 occurs in *E. coli* before purification, the absence of signal in point mutant SIRT6 indicates that mono-ADP-ribosylation depends on the catalytic activity of mSIRT6.

Having confirmed mono-ADP-ribosylation as the nature of the modification of mSIRT6, we wished to ascertain whether this modification was catalyzed in an inter- or intra-molecular fashion. mSIRT6 and two different mutants (H133Y and S56A) were used in a molecular cis/trans test for enzymatic activity. GST-mSIRT6 was purified from *E. coli* and incubated in combination with His_6-tagged mutant and wild-type mSIRT6 in the presence of [^{32}P]NAD. Reactions were purified as described before and subjected to autoradiography. Labeled GST-mSIRT6 migrated as an ~80-kDa band in all reactions (Fig. 6*B*). His_6-tagged mSIRT6 migrated as a strongly labeled 39-kDa band (Fig. 6*B*). However, this band was absent from the corresponding reactions of both His_6-tagged mutants, demonstrating that GST-mSIRT6 was unable to ADP-ribosylate those proteins. Coomassie Blue staining of the gel prior to film exposure revealed similar amounts of protein in all three lanes (data not shown). We therefore conclude that the auto-ADP-ribosylation reaction catalyzed by mSIRT6 is intra-molecular.

DISCUSSION

Here we provide the first characterization of a class IV sirtuin, mouse SIRT6. This sirtuin shows a relatively weak sequence homology to the yeast Sir2 (25%), suggesting a significant divergence in function and enzymatic activity. Consistent with published findings, we failed to detect any NAD-dependent protein deacetylase activity in preparations of mSIRT6 expressed in bacterial and mammalian cells. Surprisingly,

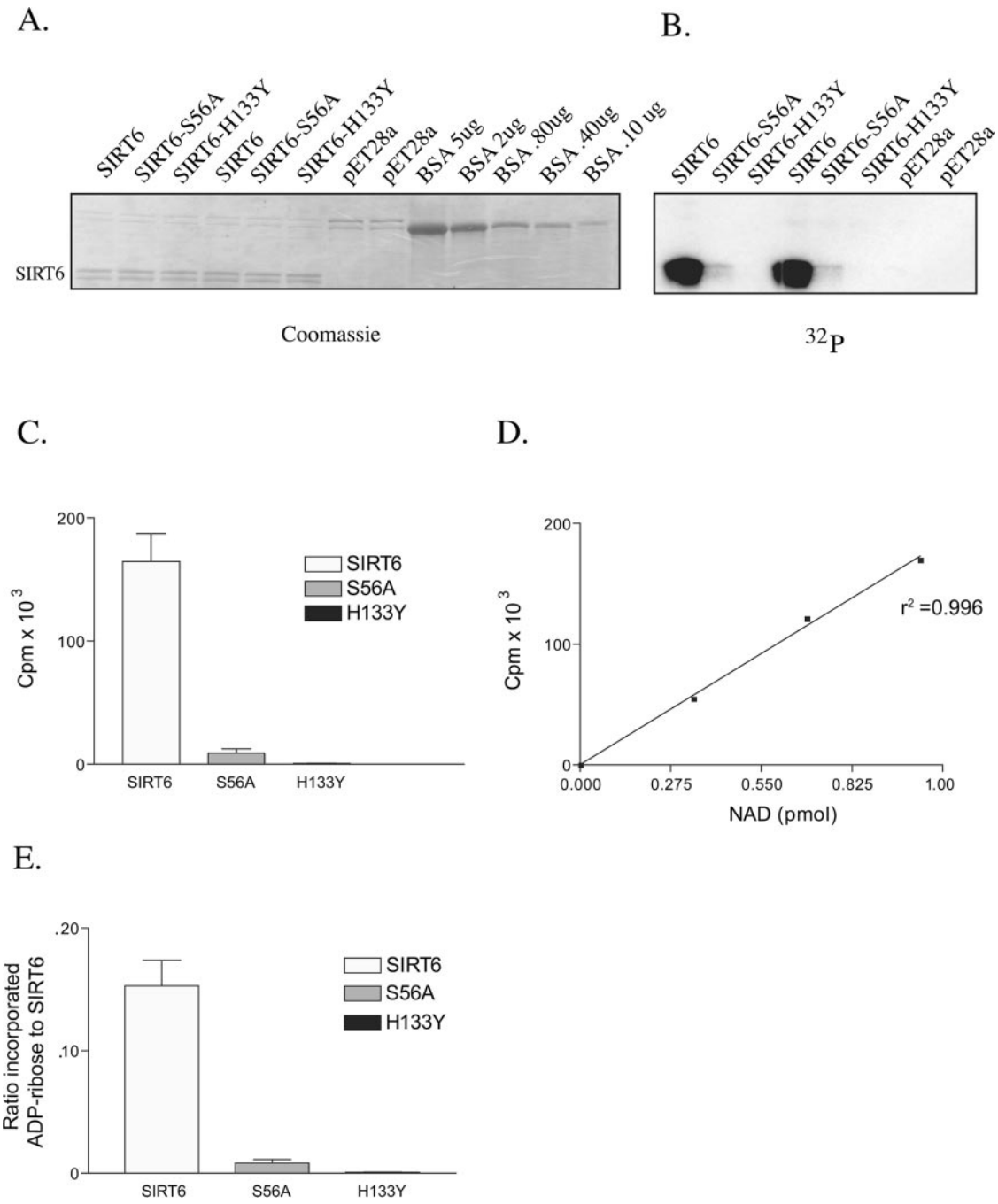

FIG. 5. **Quantification of auto-ADP-ribosylation by mSIRT6.** *A*, 0.5 μl of recombinant wild-type SIRT6 and two mutant forms (S56A and H133Y) were incubated with [^{32}P]NAD, purified by gel filtration chromatography, and analyzed by SDS-PAGE. The gel was stained with Coomassie Blue and photographed. SIRT6 quantities were determined by comparison to bovine serum albumin standards run on the same gel. Wild-type SIRT6 was estimated at 0.250 μg, or 6.4 pmol. *B*, the stained gel from *A* was analyzed by autoradiography to confirm radiolabeling of SIRT6. *C*, SIRT6 bands were excised from the gel, and ^{32}P radioactivity was quantitated by scintillation counting. Results are normalized to measurements from the corresponding region excised from pET28a vector control lanes. *D*, a NAD standard curve was generated by scintillation counting of known quantities of [^{32}P]NAD diluted to reflect the ratio of unlabeled NAD to [^{32}P]NAD in the reaction. *E*, ratio of incorporated ADP-ribose to SIRT6 was determined as follows. Radioactivity measured in SIRT6 bands was converted to pmol of NAD by comparison with the standard curve. That quantity (pmol of NAD) was divided by pmol of SIRT6 to attain the fraction of labeled mSIRT6.

mSIRT6 did show a robust ADP-ribosyltransferase activity *in vitro*, indicating that recombinant bacterial preparations indeed contained active protein.

We conclude that mSIRT6 is a mono-ADP-ribosyltransferase for the following reasons. First, the purified protein can catalyze the transfer of radiolabel from [^{32}P]NAD, a reaction also catalyzed by other Sir2 family members (17, 19, 22) and previously shown to be mono-ADP-ribosylation (19). Second, this activity requires the catalytic function of mSIRT6 because two different point mutations in phylogenetically invariant residues predicted to abolish enzymatic activity eliminated the transfer of label from NAD to mSIRT6. Third, only the enzymatically modified form of mSIRT6 is recognized by an anti-ADP-ribose antibody specific to mono-ADP-ribosylated proteins. Finally, the transfer of label from [^{32}P]NAD to mSIRT6 is accomplished by an intra-molecular mechanism, indicating that SIRT6 may use ADP-ribosylation as a way to auto-regulate its activity.

Recombinant mSIRT6 expressed in *E. coli* and incubated with NAD was able to incorporate a quantity of ADP-ribose

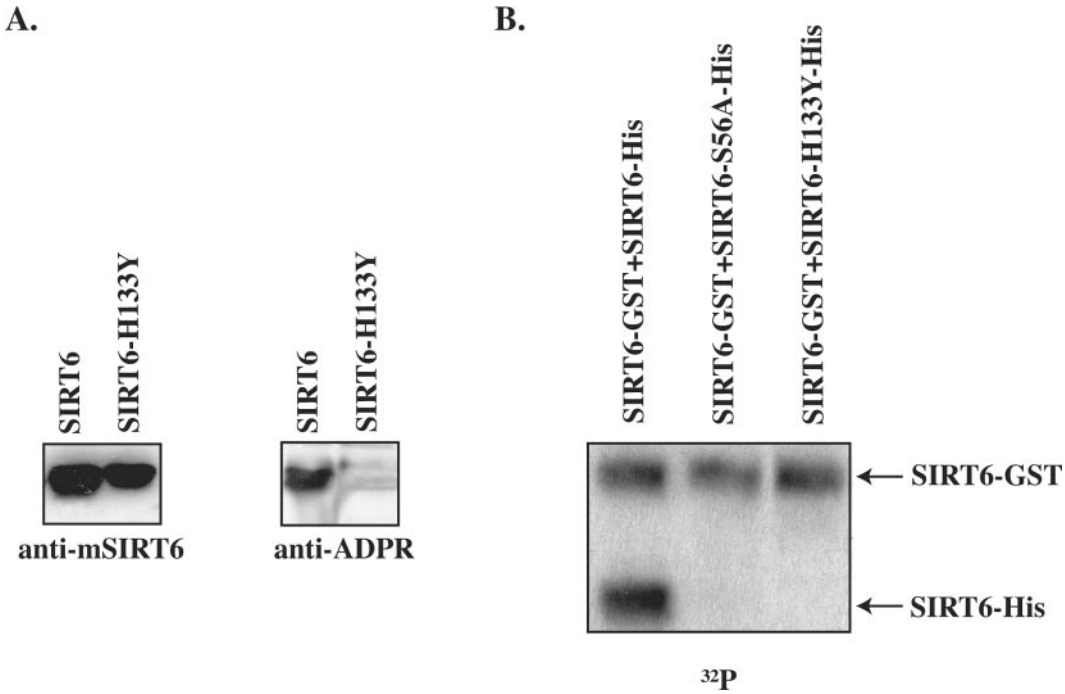

FIG. 6. **Auto-ADP-ribosylation of mSIRT6.** *A*, equal amounts of recombinant mSIRT6 and mutant mSIRT6-H133Y protein were incubated with [^{32}P]NAD$^+$ and blotted to nitrocellulose as described in the Fig. 4 legend. The blot was probed with antibody specific to mono-ADP-ribose, stripped, and reprobed with antibody specific to mSIRT6 as a control. *B*, GST-SIRT6 was incubated with [^{32}P]NAD$^+$ and either mSIRT6 (*lane 1*), mSIRT6-S56A (*lane 2*), or mSIRT6-H133Y (*lane 3*). Reactions were analyzed by autoradiography as described in the legend to Fig. 4*C*. Coomassie Blue staining of the gel prior to film exposure revealed similar amounts of recombinant protein in all three lanes (data not shown).

equivalent to 15% of the moles of mSIRT6 present in the reaction. This level of ADP-ribosylation is impressive, considering the intra-molecular nature of the reaction, by which a molecule of SIRT6 is only active on a single substrate molecule. We failed to observe a band shift resulting from ADP-riboysla-tion, suggesting that the number of amino acid residues ADP-ribosylated on mSIRT6 is very small. Assuming a single ADP-ribosylation per molecule of SIRT6, our results indicate a strong 15% activity in our recombinant protein preparations.

Mouse SIRT6 is broadly expressed at the RNA and protein levels throughout development and during adulthood in at least eight different tissue types, indicating broad expression throughout the organism. The SIRT6 protein is particularly abundant in brain and liver. Interestingly, mSIRT6 protein expression is highest in muscle, even though mRNA levels in this tissue are low relative to those of actin. This might indicate increased SIRT6 protein stability in muscle compared with other tissue types. Alternatively, the disproportionate amount of SIRT6 protein observed in muscle may result from an increased rate of translation of SIRT6 mRNA in this tissue type.

Localization studies of mSIRT6 using N- and C-terminal GFP fusions as well as antibodies to two different epitopes showed that expression of mSIRT6 was largely nuclear, with only a diffuse presence in cytoplasm. Interestingly, endogenous levels of SIRT6 do not permeate certain intra-nuclear regions, probably corresponding to the nucleolus (Fig. 3*B*). The only other mouse class IV sirtuin, mSIRT7, is localized to the nucleolus.[2] We therefore speculate that mSIRT6 and mSIRT7, despite extensive sequence homology (39%), have non-overlapping functions within the cell. Like SIRT6, SIRT7 has not been shown to possess any *in vitro* protein deacetylase activity (15).

Several ADP-ribosyltransferases are capable of reversible auto-modification resulting in altered enzymatic activity. *Pseudomonas* ExoS, a bifunctional enzyme, is a Rho GTPase-activating protein as well as an ADP-ribosyltransferase (25). Auto-ADP-ribosylation at arginine 146, observed *in vitro* and *in vivo*, reduces GTPase-activating protein activity (25), suggesting a mechanism for intra-molecular regulation. In mammals, auto-modification of ADP-ribosyltransferase 5 converts the protein from NADase to transferase (26), again suggesting a mechanism for regulation of enzyme activity. We speculate that SIRT6 might regulate its own activity *in vivo* by ADP-ribosylation of specific residues required for activity. At this time, we have not yet identified the physiological targets of SIRT6. Unlike class I sirtuins including yeast Sir2 and SIRT1, SIRT6 appears to be highly specific *in vitro*, even failing to catalyze ADP-ribosylation of SIRT6 molecules in trans. The discovery of auto-ADP-ribosyltransferase activity in preparations of recombinant mouse SIRT6 is the first report of enzymatic activity for any class IV sirtuin. Future experiments will aim to identify physiological substrates ADP-ribosylated by SIRT6.

Acknowledgments—We thank H. Hilz (Hamburg, Germany) for the ADP-ribose antibody. We also thank Laura Bordone (Guarente laboratory, Massachusetts Institute of Technology) for the kind contribution of mouse tissue protein samples. Finally, we thank Marcia Haigis and Gil Blander for scientific input and critical discussions.

REFERENCES

1. Blander, G., and Guarente, L. (2004) *Annu. Rev. Biochem.* **73,** 417–435
2. Gasser, S. M., and Cockell, M. M. (2001) *Gene* (*Amst.*) **279,** 1–16
3. Hekimi, S., and Guarente, L. (2003) *Science* **299,** 1351–1354
4. Bitterman, K. J., Medvedik, O., and Sinclair, D. A. (2003) *Microbiol. Mol. Biol. Rev.* **67,** 376–399
5. Kaeberlein, M., McVey, M., and Guarente, L. (1999) *Genes Dev.* **13,** 2570–2580
6. Lin, S. J., Ford, E., Haigis, M., Liszt, G., and Guarente, L. (2004) *Genes Dev.* **18,** 12–16
7. Lin, S. J., Defossez, P. A., and Guarente, L. (2000) *Science* **289,** 2126–2128
8. Rogina, B., and Helfand, S. L. (2004) *Proc. Natl. Acad. Sci. U. S. A.* **101,** 15998–16003
9. Wood, J. G., Rogina, B., Lavu, S., Howitz, K., Helfand, S. L., Tatar, M., and Sinclair, D. (2004) *Nature* **430,** 686–689
10. Tissenbaum, H. A., and Guarente, L. (2001) *Nature* **410,** 227–230
11. North, B. J., and Verdin, E. (2004) *Genome Biol.* **5,** 224
12. Motta, M. C., Divecha, N., Lemieux, M., Kamel, C., Chen, D., Gu, W., Bultsma, Y., McBurney, M., and Guarente, L. (2004) *Cell* **116,** 551–563

[2] E. Ford and L. Guarente, unpublished data.

13. Brunet, A., Sweeney, L. B., Sturgill, J. F., Chua, K. F., Greer, P. L., Lin, Y., Tran, H., Ross, S. E., Mostoslavsky, R., Cohen, H. Y., Hu, L. S., Cheng, H. L., Jedrychowski, M. P., Gygi, S. P., Sinclair, D. A., Alt, F. W., and Greenberg, M. E. (2004) *Science* **303,** 2011–2015
14. Picard, F., Kurtev, M., Chung, N., Topark-Ngarm, A., Senawong, T., Machado De Oliveira, R., Leid, M., McBurney, M. W., and Guarente, L. (2004) *Nature* **429,** 771–776
15. North, B. J., Marshall, B. L., Borra, M. T., Denu, J. M., and Verdin, E. (2003) *Mol. Cell* **11,** 437–444
16. Sauve, A. A., and Schramm, V. L. (2004) *Curr. Med. Chem.* **11,** 807–826
17. Frye, R. A. (1999) *Biochem. Biophys. Res. Commun.* **260,** 273–279
18. Tanner, K. G., Landry, J., Sternglanz, R., and Denu, J. M. (2000) *Proc. Natl. Acad. Sci. U. S. A.* **97,** 14178–14182
19. Tanny, J. C., Dowd, G. J., Huang, J., Hilz, H., and Moazed, D. (1999) *Cell* **99,** 735–745
20. Tanny, J. C., and Moazed, D. (2001) *Proc. Natl. Acad. Sci. U. S. A.* **98,** 415–420
21. Armstrong, C. M., Kaeberlein, M., Imai, S. I., and Guarente, L. (2002) *Mol. Biol. Cell* **13,** 1427–1438
22. Imai, S., Armstrong, C. M., Kaeberlein, M., and Guarente, L. (2000) *Nature* **403,** 795–800
23. Frye, R. A. (2000) *Biochem. Biophys. Res. Commun.* **273,** 793–798
24. Corda, D., and Di Girolamo, M. (2003) *EMBO J.* **22,** 1953–1958
25. Riese, M. J., Goehring, U. M., Ehrmantraut, M. E., Moss, J., Barbieri, J. T., Aktories, K., and Schmidt, G. (2002) *J. Biol. Chem.* **277,** 12082–12088
26. Weng, B., Thompson, W. C., Kim, H. J., Levine, R. L., and Moss, J. (1999) *J. Biol. Chem.* **274,** 31797–31803
27. Kain, S. R., Mai, K., and Sinai, P. (1994) *BioTechniques* **17,** 982–987
28. Finnin, M. S., Donigian, J. R., and Pavletich, N. P. (2001) *Nat. Struct. Biol.* **8,** 621–625
29. Zhang, J., and Snyder, S. H. (1992) *Proc. Natl. Acad. Sci. U. S. A.* **89,** 9382–9385
30. Itoga, M., Tsuchiya, M., Ishino, H., and Shimoyama, M. (1997) *J. Biochem.* (*Tokyo*) **121,** 1041–1046
31. Meyer, T., and Hilz, H. (1986) *Eur. J. Biochem.* **155,** 157–165